# Bioimaging and Biodistribution of the Metal-Ion-Controlled Self-Assembly of $PYY_{3-36}$ Studied by SPECT/CT

Panagiota Kalomoiri,[a] Cristina Rodríguez-Rodríguez,[b, c] Kasper K. Sørensen,[a] Marta Bergamo,[b] Katayoun Saatchi,[b] Urs O. Häfeli,*[b, d] and Knud J. Jensen*[a]

The controlled self-assembly of peptide- and protein-based pharmaceuticals is of central importance for their mode of action and tuning of their properties. Peptide $YY_{3-36}$ ($PYY_{3-36}$) is a 36-residue peptide hormone that reduces food intake when peripherally administered. Herein, we describe the synthesis of a $PYY_{3-36}$ analogue functionalized with a metal-ion-binding 2,2′-bipyridine ligand that enables self-assembly through metal complexation. Upon addition of $Cu^{II}$, the bipyridine-modified $PYY_{3-36}$ peptide binds stoichiometric quantities of metal ions in solution and contributes to the organization of higher-order assemblies. In this study, we aimed to explore the size effect of the self-assembly *in vivo* by using non-invasive quantitative single-photon emission computed tomography/computed tomography (SPECT/CT) imaging. For this purpose, bipyridine-modified $PYY_{3-36}$ was radiolabeled with a chelator holding $^{111}In^{III}$, followed by the addition of $Cu^{II}$ to the bipyridine ligand. SPECT/CT imaging and biodistribution studies showed fast renal clearance and accumulation in the kidney cortex. The radiolabeled bipyridyl-$PYY_{3-36}$ conjugates with and without $Cu^{II}$ presented a slightly slower excretion 1 h post injection compared to the unmodified-$PYY_{3-36}$, thus demonstrating that higher self-assemblies of the peptide might have an effect on the pharmacokinetics.

## Introduction

The oligomeric state of peptide- and protein-based pharmaceuticals is critical for their mode of action.[1] It has been estimated that about one third of cellular proteins are oligomeric,[2] and both hydrophobic and polar interactions, as well as metal-ion coordination, are key factors in their ability to self-assemble. Native self-assemblies are driven by oligomerization, in response to external conditions, and are formed reversibly. Coordination with metal ions can induce conformational changes in the peptides that can modulate their properties and function.[3,4] Examples of metal-ion-induced self-assembly include the copper-mediated homodimerization of the HAH1 metallochaperone,[5] the monomer/tetramer equilibrium of lacto-transferrin,[6] or the highly stabilized zinc-binding hexamers of insulin.[7] Using natural self-assemblies as a guide, the introduction of non-native methods, such as abiotic metal-ligand residues on peptides, can cause higher-order self-assemblies and controlled oligomerization.[8]

Metal-ion-binding ligands such as bipyridine, terpyridine, nitrilotriacetic acid and pyridine have been widely used as a strategy to induce conformational changes and modulate peptide properties in the presence of metal ions ($Fe^{II}$, $Cu^{II}$, $Co^{II}$, $Ni^{II}$, $Ru^{II}$ and $Zn^{II}$).[8] Multidentate chelating ligands demonstrate significantly higher binding affinities for metal ions than several monodentate ligands combined (this is known as the chelation effect).[9] In this study, we used the nitrogen-containing heterocyclic ligand 2,2′-bipyridine (bipy), which has the ability to coordinate various transition metal ions.[10] Bipy has previously been introduced into peptides to enable the formation of collagen-based three-dimensional networks,[11–13] intramolecular directing and folding of artificial metalloproteins[14] and structural changes such as coiled coils in small peptides.[15–17] Previously, we demonstrated that the insulin variant InsX2 modified with bipy formed the first published trimers of insulin upon the addition of $Fe^{II}$.[18] For intermolecular self-assembly, bipy groups function as bidentate ligands with predictable binding affinities towards transition metal ions.[8] Gilmartin and co-workers attached three bipy ligands on peptide nucleic acids (PNA), which could coordinate with either two or three metal ions ($Fe^{II}$ and $Cu^{II}$, respectively) to form two different duplex structures.[19] Coppock and collaborators synthesized a heterofunctional artificial tripeptide that contained three pendant ligands, pyridine, methyl pyridine and terpyridine, and self-assembled into an antiparallel duplex by coordination of three $Cu^{II}$ ions.[20] Our strategy is to control peptide quaternary structure by selective introduction of a bipy ligand to the peptide $YY_{3-36}$ ($PYY_{3-36}$), which enables self-assembly through metal-ion coordination.

[a] P. Kalomoiri, Dr. K. K. Sørensen, Prof. K. J. Jensen
Center for Biopharmaceuticals and Biobarriers in Drug Delivery
Department of Chemistry, University of Copenhagen
Thorvaldsensvej 40, 1871 Frederiksberg (Denmark)
E-mail: kjj@chem.ku.dk
[b] Dr. C. Rodríguez-Rodríguez, M. Bergamo, Dr. K. Saatchi, Prof. U. O. Häfeli
Faculty of Pharmaceutical Sciences, University of British Columbia
2405 Wesbrook Mall, Vancouver, BC V6T 1Z3 (Canada)
E-mail: urs.hafeli@ubc.ca
[c] Dr. C. Rodríguez-Rodríguez
Department of Physics and Astronomy, University of British Columbia
6224 Agricultural Road, Vancouver, British Columbia V6T 1Z1 (Canada)
[d] Prof. U. O. Häfeli
Center for Drug Delivery and Biophysics of Biopharmaceuticals
Department of Pharmacy, Faculty of Health and Medical Sciences
University of Copenhagen
Universitetsparken 2, 2100 Copenhagen (Denmark)

Supporting information for this article is available on the WWW under https://doi.org/10.1002/cbic.202000266

$PYY_{3-36}$ belongs to the neuropeptide (NPY) family of peptides (the sequences are listed in Table 1), that mediate their effect through four receptors, the Y1, Y2, Y4 and Y5.[9] Full-length PYY ($PYY_{1-36}$) is released postprandially by gastrointestinal L-cells in proportion to nutrient-level, after which it is rapidly truncated to the 34 amino acid peptide, $PYY_{3-36}$, by dipeptidyl-peptidase IV (DPP-IV).[21] Peripheral administration of $PYY_{3-36}$ reduces food intake in both lean and obese humans, acting through Y2 receptors.[22,23]

In recent years, $PYY_{3-36}$ analogues have again become interesting as potential anti-obesity therapeutics.[24] Anti-obesity $PYY_{3-36}$ therapeutics are actively investigated,[25–28] but the short circulatory half-life of ~10 min and the less than ideal Y2R selectivity of native $PYY_{3-36}$ over the other neuropeptide Y receptors,[29,30] renders their development challenging. One approach to overcome the short systemic half-life and provide a prolonged mode-of-action is to construct higher-order $PYY_{3-36}$ assemblies.[31,32] The therapeutically very successful long-acting insulin, insulin degludec, has a fatty diacid derivatization and is formulated with phenol and $Zn^{II}$. Upon subcutaneous injection it forms an oligomeric depot that slowly releases monomers for absorption, thus providing an extended duration of action.[33] This inspired us to aim for a metal ion mediated assembly and disassembly in a subcutaneous depot.

**Table 1.** Sequences of human NPY, $PYY_{1-36}$ and $PYY_{3-36}$.

| Peptide | Sequence |
|---|---|
| NPY | YPSKPDNPGEDAPAEDMARYYSALRHYINLITRQRY-$NH_2$ |
| $PYY_{1-36}$ | YPIKPEAPGEDASPEELNRYYASLRHYLNLVTRQRY-$NH_2$ |
| $PYY_{3-36}$ | IKPEAPGEDASPEELNRYYASLRHYLNLVTRQRY-$NH_2$ |

In this study, we aimed to design a $PYY_{3-36}$ analogue with one distinct metal-ion binding site, bipy, enabling self-assembly through coordination with $Cu^{II}$. To investigate the effects of the self-assembly in a biodistribution context, we performed *in vivo* studies in mice using non-invasive quantitative single-photon emission computed tomography/computed tomography (SPECT/CT) imaging (Figure 1). For this purpose, the peptide was modified with a bifunctional chelator, *S*-2-(4-isothiocyanatobenzyl)diethylenetriamine pentaacetic acid (*p*-SCN–Bn-DTPA) and was radiolabeled with $^{111}In^{III}$. The radiolabeled peptide was then reacted with $Cu^{II}$ for coordination to the bipy ligand of the $PYY_{3-36}$ analogue (Figure 1). $^{111}In^{III}$ facilitated the *in vivo* imaging and tracking of the peptide, while $Cu^{II}$ promoted the formation of the self-assembly.

## Results and Discussion

### Design and synthesis of $PYY_{3-36}$ analogues

To study the formation of different peptide self-assemblies, we re-engineered $PYY_{3-36}$ by conjugating bipy, which enables self-assembly by metal-ion coordination.[34] Bipy was chosen as it is a well-characterized metal-binding abiotic ligand that has been used to prepare different supramolecular assemblies.[35] $Cu^{II}$ was used as the first-row transition metal ion because it exhibits a high binding affinity for bipy (for thermodynamic parameters from the literature, see Table S1).[36,37] Another rationale for choosing $Cu^{II}$ as the metal ion was the possibility of using $^{64}Cu$ for future positron emission tomography (PET) imaging studies. Here, the $^{64}Cu$ would have a dual role by inducing the self-assembly of the peptide and also being a γ-emitting radio-

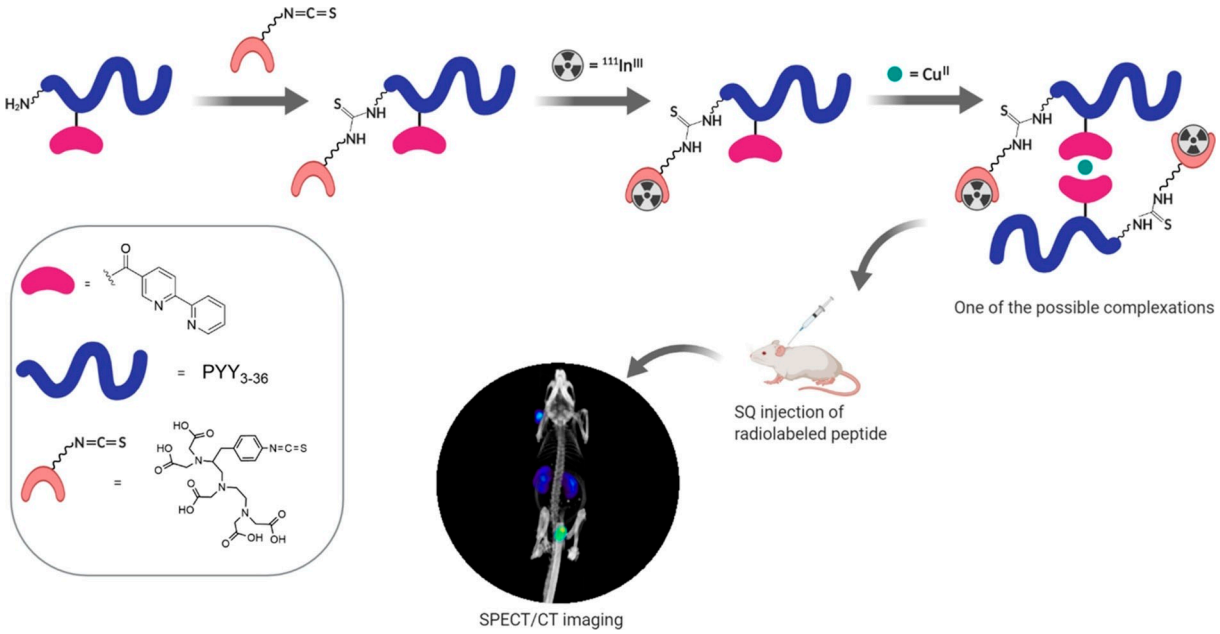


**Figure 1.** Overview of the experimental design. Bipyridyl-$PYY_{3-36}$ was N-terminally modified by formation of a thiourea bond through reaction with *p*-SCN–Bn-DTPA. It was then radiolabeled with $^{111}In^{III}$, and the radiolabeled peptide was treated with $Cu^{II}$ to form higher-order assemblies. The radioconjugate was further studied *in vivo* by using SPECT/CT.

isotope. Moreover, Cu is the third most abundant trace transition metal in the human body with a normal content of 1.4–2.1 mg/kg.[38] As a model peptide, we chose an analogue of native $PYY_{3-36}$ (Table 1), $[R^4,K^7,W^{30}]PYY_{3-36}$. Position 7 was selected as the site of modification due to the minimal loss of activity when modified.[25–27] Also, tryptophan substitution in position 30 was performed as it has been shown to increase selectivity and maintain $Y_2$ receptor affinity.[28]

The peptide was assembled by Fmoc/*t*Bu strategy using automated solid-phase peptide synthesis (SPPS) on Rink Amide TentaGel resin to obtain an amidated C terminus (Scheme 1). To ensure selectivity, the N-terminal α-amino group was protected with the base-stable *tert*-butyloxycarbonyl (Boc) group. Site-specific acylation on solid phase was achieved by using the orthogonal allyloxycarbonyl (Alloc) protection group at the $N^{\varepsilon}$-Lys at position 7. The Alloc group can be selectively removed by tetrakis(triphenylphosphine)palladium(0) ($(PPh_3)_4Pd(0)$) in the presence of the borane dimethylamine complex ($(CH_3)_2NH{\cdot}BH_3$) to release the free amino group.[39] The bipy carboxylic acid was activated by *N,N,N′,N′*-tetramethyl-*O*-(*N*-succinimidyl)uronium tetrafluoroborate (TSTU) and *N,N*-diisopropylethylamine (DIEA) and then it was coupled on-resin to the free Lys $N^{\varepsilon}$-amine to give $[R^4,K^7(bipy),W^{30}]PYY_{3-36}$ (hereafter referred to as $PYY_{3-36}$-bipy). The acetylated peptide (hereafter referred to as $PYY_{3-36}$-Ac), which was subsequently used as a control, was obtained by on-resin acetylation with acetic anhydride ($Ac_2O$; Scheme 1). Peptides were analyzed by analytical reversed-phase high-performance liquid chromatography (RP-HPLC) coupled to electrospray ionization mass spectrometry (ESI-MS). Purification was conducted using RP-HPLC. Analytical data are presented in Table S2.

### Metal-binding properties of $PYY_{3-36}$ analogues

In order to study the metal ion coordination of the modified $PYY_{3-36}$ peptides with $Cu^{II}$, reactions with different equivalents of $Cu^{II}$ were carried out for both modified peptides: $PYY_{3-36}$-bipy and $PYY_{3-36}$-Ac. Both peptides showed absorption maxima at around 280 nm, due to the aromatic tryptophan and tyrosine residues on the peptide chain. Upon addition of different equivalents of $Cu^{II}$ in solution, $PYY_{3-36}$-bipy revealed a significant bathochromic shift at about 300/320 nm due to the coordination of the bipy ligand to the metal ion (Figure 2A), this is consistent with previously reported data.[40] The observation of isosbestic points in the near UV area around 272 and 302 nm of the UV/vis suggests the existence of at least two species in solution and therefore, an equilibrium reaction. $PYY_{3-36}$-Ac (Figure 2B) did not show any spectral changes, which is indicative of no coordination.

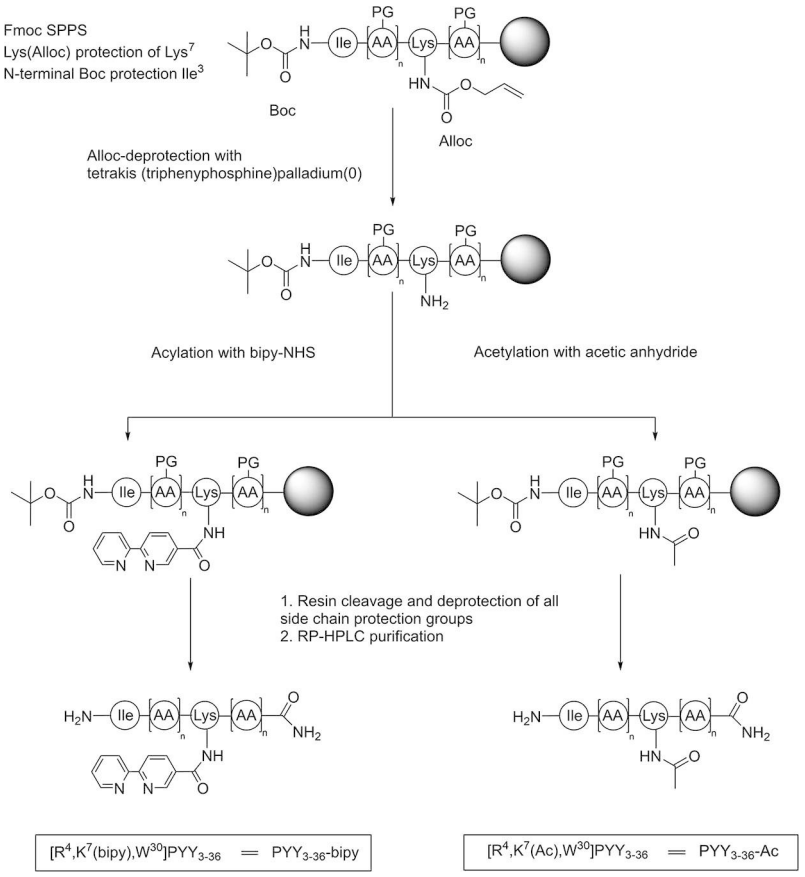


**Scheme 1.** On-resin modification of $PYY_{3-36}$ analogues (amines are implicit in the one- and three-letter code for amino acids, but here they are shown explicitly for added clarity).

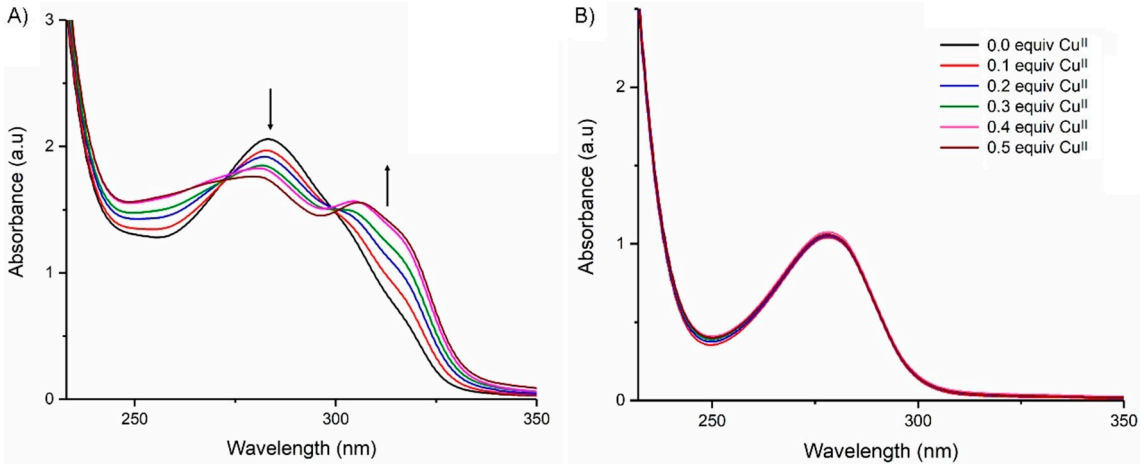


**Figure 2.** UV/vis absorbance spectra of the titration of A) $PYY_{3-36}$-bipy (100 μM) and B) $PYY_{3-36}$-Ac (100 μM) with increasing equivalents of $Cu^{II}$ in 0.1 mM PBS buffer (pH 7).

### Dynamic light scattering

The assembly of $PYY_{3-36}$-bipy (100 μM) was monitored by dynamic light scattering (DLS) upon addition of 0–0.5 equiv. of $Cu^{II}$ (Figure 3a). In the absence of $Cu^{II}$, $PYY_{3-36}$-bipy displayed a large assembly (75 nm radius) indicating an aggregation of multiple $PYY_{3-36}$-bipy molecules even in the absence of metal ions, possibly due to interactions between the bipy ligands. Upon the addition of increasing equivalents of $Cu^{II}$ to $PYY_{3-36}$-bipy (Figure 3A), the formation of larger assemblies was observed. This suggested that the presence of $Cu^{II}$ facilitated higher-order assemblies (radii from 80 to 150 nm). In the case of the acetylated control, a hydrodynamic radius of approximately 2 nm was observed, which remained constant with increasing concentrations of $Cu^{II}$. The above data indicate that the addition of $Cu^{II}$ facilitates higher-order self-assemblies through bipy coordination. Chmielewski and coworkers had investigated the self-assembly of bipyridyl-modified collagen peptides with the metals $Fe^{II}$, $Cu^{II}$, $Zn^{II}$ and $Ni^{II}$ and only $Fe^{II}$ and $Cu^{II}$ were found to promote the assembly of the bipy-collagen-mimetic peptide.[12]

### Radiolabeling of $PYY_{3-36}$ analogues

In order to evaluate the pharmacokinetics and biodistribution of the self-assembled $PYY_{3-36}$ *in vivo*, $PYY_{3-36}$-bipy and $PYY_{3-36}$-Ac were conjugated N-terminally to the bifunctional chelator *p*-SCN–Bn-DTPA (Scheme 2a). Bifunctional chelators (BFCs) are chelators that can bind a radiometal and have a reactive functional group for covalent attachment to any vector (e.g., peptides, antibodies, nanoparticles).[41] The isothiocyanate derivate of DTPA was chosen as it can be radiolabeled with various radiometal ions at room temperature within a few minutes.[42] Also, one advantage of the isothiocyanate derivative is that it can be conjugated to the peptide through the carbon

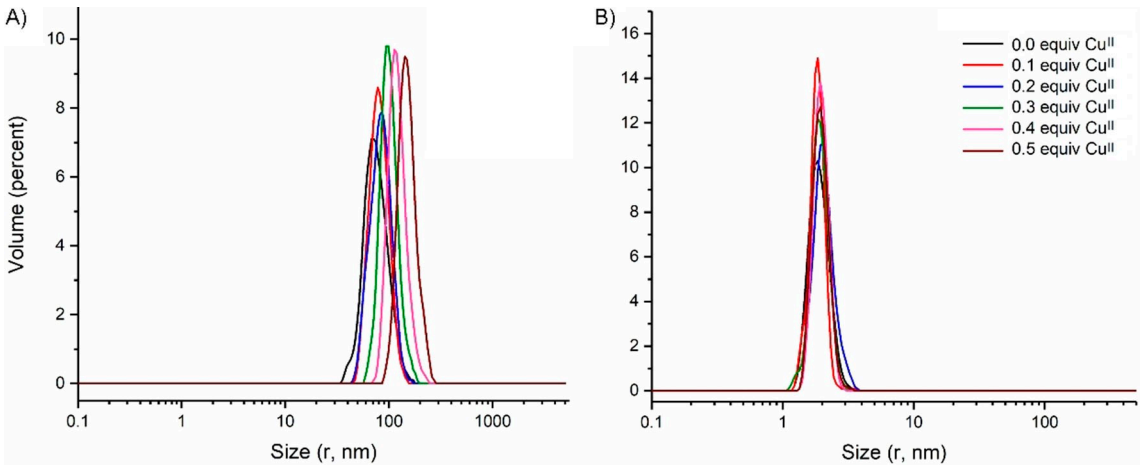


**Figure 3.** Dynamic light scattering of A) $PYY_{3-36}$-bipy (100 μM) and B) $PYY_{3-36}$-Ac (100 μM) with increasing equivalents of $Cu^{II}$ in 0.1 mM PBS buffer (pH 7).

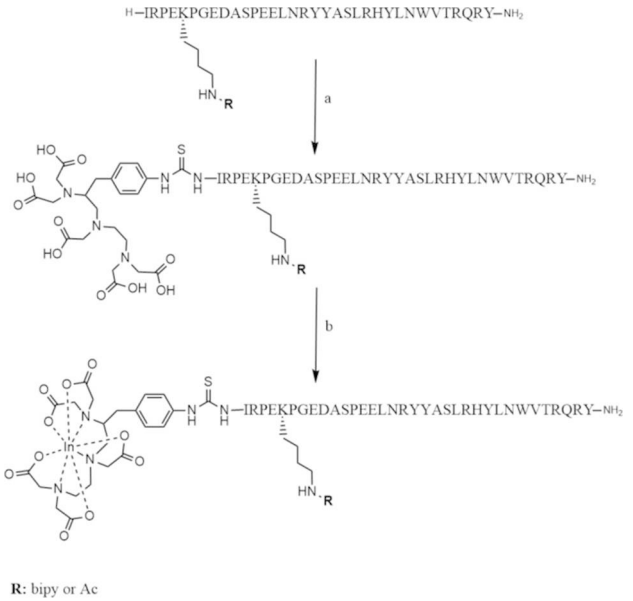


**Scheme 2.** Synthesis of $^{111}$In-DTPA-PYY$_{3-36}$ radioconjugates. a) *p*-SCN–Bn-DTPA, 30% MeCN in 0.1 M $NaHCO_3$ pH 9 at room temperature, overnight, 70% and b) $^{111}InCl_3$, $H_2O$ pH 6, 25 °C, 1 h, 600 rpm.

backbone and side-arm functionalization without blocking one of the coordinating carboxylate arms.[43,44] Regarding the N-terminal modification, an alanine scan study to PYY$_{3-36}$ showed that substitutions in the N-terminal were well tolerated and led only to a minor loss of efficacy.[45] Another study showed that lipidation in the N-terminal with a $C_{18}$ acid-γGlu reached approximately 80% of PYY$_{3-36}$'s maximal efficacy to the Y2 receptor.[46] PYY$_{3-36}$-bipy and PYY$_{3-36}$-Ac were modified N-terminally at pH 9 by formation of a thiourea bond through reaction with *p*-SCN–Bn-DTPA. After overnight incubation, the modified PYY-chelator conjugates were purified and analyzed by RP-HPLC (Figure 4A and B).

Radiolabeling of DTPA-PYY$_{3-36}$-bipy and DTPA-PYY$_{3-36}$-Ac was then carried out with $^{111}InCl_3$ (Scheme 2b). Indium-111 has a physical half-life of 2.806 days,[47] which is suitable for investigating our tracer pharmacokinetics *in vivo* over a long time range. It emits photons with multiple energies (X-rays: 22–27 keV: 82.8%, 171 keV: 90.7%, and 245 keV: 94.1%)[48] and is thus useful for SPECT diagnostic imaging.

In the current study, the radiolabeling of DTPA-PYY$_{3-36}$-bipy and DTPA-PYY$_{3-36}$-Ac was performed at room temperature with $^{111}InCl_3$ (41.44 MBq) in water (850 and 400 μL respectively, 0.13 mg/mL) over 1 hour and produced $^{111}$In-labeled peptides at a radiochemical yield of >95% as confirmed by radio-HPLC. The radioconjugates eluted with the same retention time ($t_R$ = 11.60 min) and peak shapes as the unmodified and chelator-modified PYY$_{3-36}$ (Figure 4). A sample of uncomplexed $^{111}InCl_3$ alone eluted early at the gradient ($t_R$ = 1.9 min; Figure S4). On instant thin-layer chromatography (ITLC) strips, the chelated $^{111}$In-DTPA-PYY$_{3-36}$-bipy and $^{111}$In-DTPA-PYY$_{3-36}$-Ac remained at the origin, while the free $^{111}In^{III}$ sample moved along with the mobile phase front (Figure S5), further supporting the radio-HPLC results. Analyses by dynamic light scattering (DLS) indicated that the hydrodynamic radius remained constant upon radioconjugation (Figure S6).

### Stability study

After radiolabeling, the potential transchelation of the radiometal complex was assessed by an *in vitro* challenge with the known chelator EDTA. EDTA (0.1 M, 10% of the total volume) was added in excess to both $^{111}$In-DTPA-PYY$_{3-36}$-bipy and $^{111}$In-DTPA-PYY$_{3-36}$-Ac and stirred for one day at 37 °C. Aliquots were analyzed by ITLC after 1 and 24 hours. The fraction of intact radioconjugates was quantified by integration of the bound fraction of $^{111}In^{III}$ on ITLC plates, where the complexed $^{111}In^{III}$ remained close at the origin ($R_f$ ~ 0), whereas the free $^{111}In^{III}$ eluted with the mobile phase front ($R_f$ ~ 1). Both radioconjugates showed good stability towards EDTA (Table 2) over the tested 24 hours.

### *In vivo* imaging

To investigate the effect of the size of the self-assembled PYY$_{3-36}$ functionalized with bipy, on the biodistribution and the pharmacokinetics, $^{111}$In-DTPA-PYY$_{3-36}$-bipy complexed with 0.5 equiv. $Cu^{II}$ (group 1) and two controls; $^{111}$In-DTPA-PYY$_{3-36}$-bipy without the addition of $Cu^{II}$ (group 2) and $^{111}$In-DTPA-PYY$_{3-36}$-Ac (group 3) were administered subcutaneously into healthy mice and imaged via SPECT/CT ($n$ = 3 per group). Static scans were performed at 0, 1, 2.5 and 6 h post injection and mice were euthanized after 24 h, where the activity in the whole carcass was measured and the *ex vivo* biodistribution study was performed. SPECT images revealed that the peptides travelled from the injection site through the bloodstream to the kidneys where they were excreted into the bladder within 1 hour (Figure 5).

By assessing the organ-specific time-activity curves for the three groups, several differences are presented in the organ uptake. Standardized uptake values (SUVs) as a function of time showed that about (21 ± 2.0)% of the radioconjugate of group 1 and (23.4 ± 2.6)% of group 2 remained in the kidneys and

**Table 2.** Radiolabeling efficiency[a] and transchelation stability with EDTA[b] of the radioconjugates.

| Radioconjugate | Labeling efficiency [%] | Transchelation stability [%] 1 h | 24 h |
|---|---|---|---|
| $^{111}$In-DTPA-PYY$_{3-36}$-bipy | 98 ± 0.1 | 95 ± 0.4 | 92 ± 1.1 |
| $^{111}$In-DTPA-PYY$_{3-36}$-Ac | 95 ± 0.5 | 91 ± 0.8 | 90 ± 0.9 |

[a] The labeling efficiency in % describes the percent bound activity from the initial activity added to the reaction. [b] The stability describes the percentage of bound $^{111}In^{III}$ after incubation with 10% EDTA at 37 °C, 600 rpm. Measurements were performed in triplicate and are reported as mean ± SD.

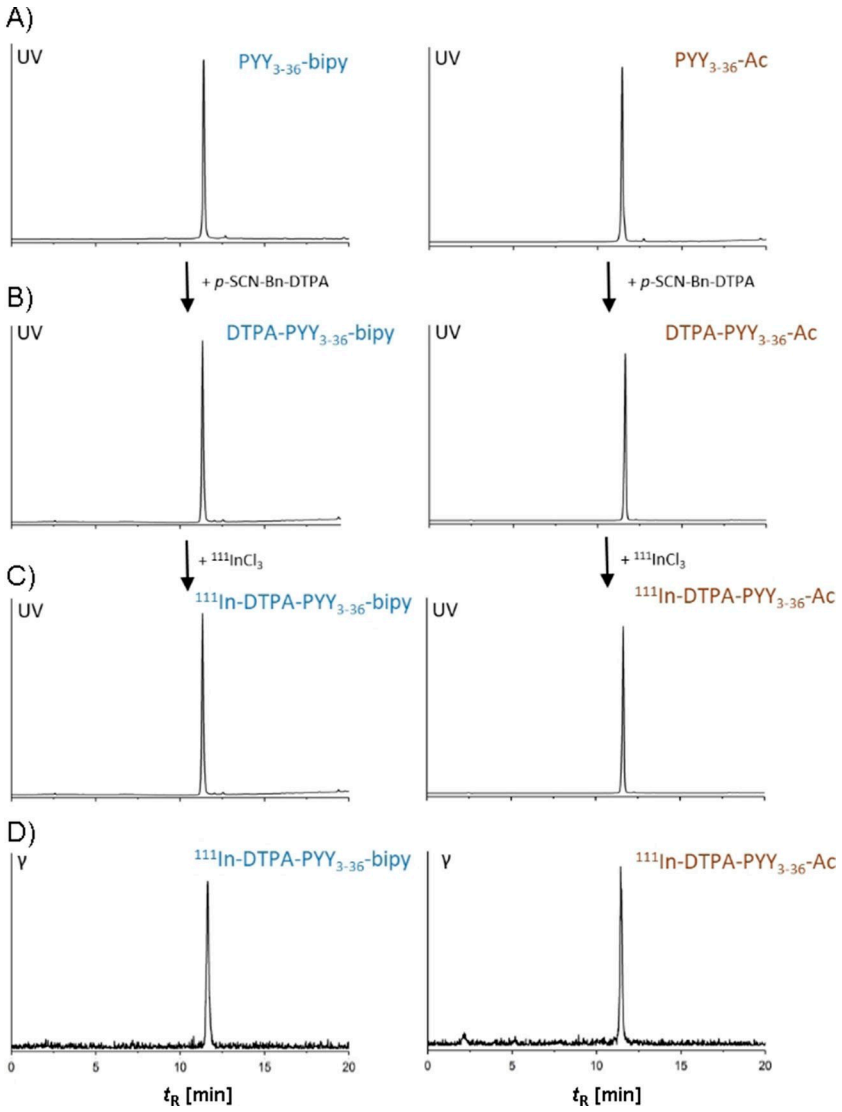


**Figure 4.** (Radio)-HPLC chromatograms of A) $PYY_{3-36}$-bipy (left) and $PYY_{3-36}$-Ac (right) as well as B) DTPA-$PYY_{3-36}$-bipy (left) and DTPA-$PYY_{3-36}$-Ac (right), C) $^{111}$In-DTPA-$PYY_{3-36}$-bipy (left) and $^{111}$In-DTPA-$PYY_{3-36}$-Ac (right) and D) radiochromatograms of $^{111}$In-DTPA-$PYY_{3-36}$-bipy (left) and $^{111}$In-DTPA-$PYY_{3-36}$-Ac (right).

injection site after 1 h and the rest was excreted via the bladder and urine (Figure 6). The radioconjugate of the acetylated group 3 was excreted slightly faster as (11.3 ± 2.5) % remained in the kidneys and injection site 1 h post injection. All three groups were cleared primarily through the renal pathway and the images showed that the activity accumulated mainly in the renal cortex rather than the medulla (Figure 5). Figure 6B depicts that the concentration of all groups in the kidney cortex remained relatively stable for 6 h.

All three $^{111}$In-DTPA-conjugated peptides showed significant localization of radioactivity in the kidney after subcutaneous administration. Elevated renal uptake and prolonged retention of $^{111}$In-DTPA-radiolabeled peptides has been observed and reported in SPECT/CT imaging and therapy.[49] Although the biggest percentage of the radiolabeled peptides was excreted into the urine 1 h post injection (Figure 6D), a small percentage was retained in the kidney cortex (Figure 6B) due to their glomerular filtration, followed by tubular reabsorption.[50] Studies have suggested that after glomerular filtration, peptides and small proteins bind to endocytic receptors at the luminal surface of the cells of the proximal tubule and are internalized.[51] It should be noted that the elevated SUV of group 2 ($^{111}$In-DTPA-$PYY_{3-36}$-bipy) at 2.5 h might be attributed to the coordination of the free bipy with another metal ion present in the kidneys. It is known that substantial amounts of iron are filtered by the kidney, but later reabsorbed to prevent deficiency.[52]

Overall, the radioactive peptide elimination was mainly through the kidneys, and less than 1% through the liver, from where it was secreted into the gallbladder within the first hour post injection. Hepatic metabolism is significantly less recurrent for most peptides than for small-molecule drugs.

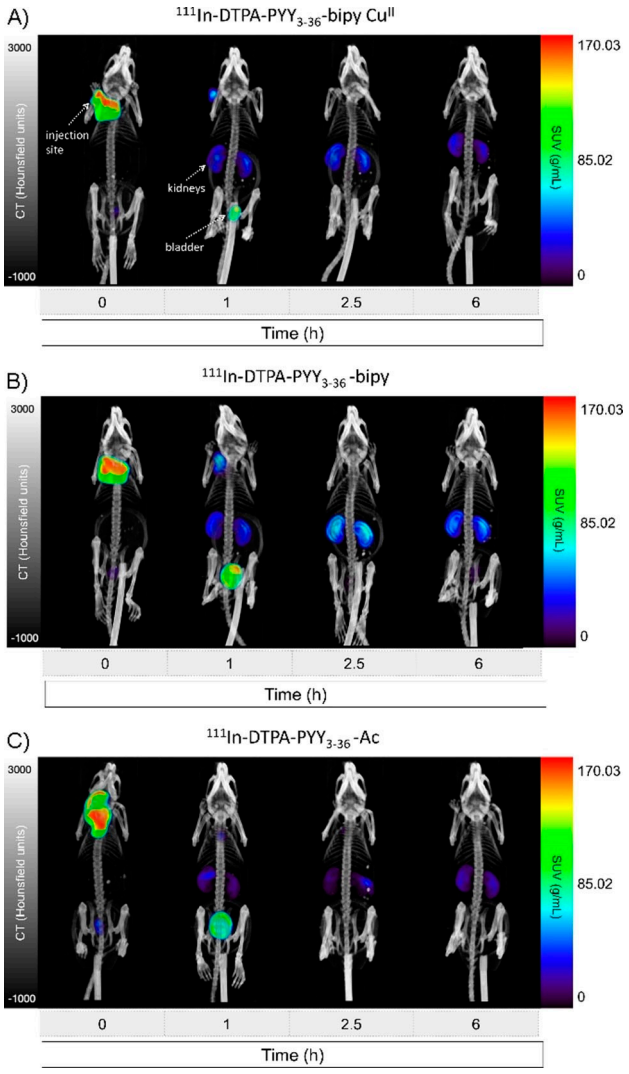


**Figure 5.** Top view maximum intensity projections (MIPs) on total body SPECT/CT scans at various time points after subcutaneous administration of A) $^{111}$In-DTPA-PYY$_{3-36}$-bipy complexed with 0.5 equiv. Cu$^{II}$, B) $^{111}$In-DTPA-PYY$_{3-36}$-bipy, and C) $^{111}$In-DTPA-PYY$_{3-36}$-Ac.

### *Ex vivo* biodistribution

The *ex vivo* biodistribution of all three $^{111}$In-labeled peptides for the major organs and tissues at 24 h post injection is presented in Figure 7. The radiolabeled peptides are mainly processed through renal clearance showing an average kidney uptake of (29.82 ± 0.39) %ID/g for group 3, (25.72 ± 1.90) %ID/g for group 2 and (17.88 ± 2.61) %ID/g for group 1. The biodistribution data confirmed the much lower liver uptake from the imaging data for all three groups. For the rest of the organs relatively similar uptakes were observed for all three peptides.

## Conclusions

In summary, we have designed and synthesized a PYY$_{3-36}$ analogue with a bidentate ligand that enabled higher-order self-assembly through coordination with Cu$^{II}$. We have demonstrated that larger metal-assisted self-assemblies were triggered by the addition of increasing concentrations of Cu$^{II}$. To investigate the *in vivo* effects of the ensemble, we conjugated the peptide with the chelator *p*-SCN–Bn-DTPA and radiolabeled this with $^{111}$In$^{III}$ to allow tracking and imaging. High-contrast SPECT/CT images and excellent visualization of the organs were obtained for all peptides. Quantitative SPECT imaging showed that the peptides were excreted predominantly via the renal pathway and less than 5% via the hepatobiliary pathway. The PYY$_{3-36}$-bipy conjugates, with and without the addition of Cu$^{II}$, presented a slightly slower excretion 1 h post injection than PYY$_{3-36}$-Ac, thus indicating that higher peptide self-assemblies might influence the pharmacokinetics. This is a first step towards the potential application of using abiotic ligands in the controlled release of biopharmaceuticals from subcutaneous depots.

## Experimental Section

### Materials

*Synthesis and purification*: Fmoc-protected amino acids, piperidine, *N,N*-diisopropylethylamine (DIEA), trifluoroacetic acid (TFA), *N*-methyl-2-pyrrolidone (NMP), diethyl ether ($Et_2O$), and *N,N*-dimethylformamide (DMF) were purchased from Iris Biotech GmbH (Marktredwitz, Germany). *N*-[(1*H*-benzotriazol-1-yl)(dimethylamino) methylene]-*N*-methylmethanaminium hexafluorophosphate *N*-oxide (HBTU) and 1-hydroxy-7-azabenzotriazol (HOAt) were purchased from GL Biochem Ltd. (Shanghai, China). Rink functionalized TentaGel S RAM (0.22 mmol/g) was purchased from Rapp Polymere GmbH (Tübingen, Germany). Acetonitrile and dichloromethane were purchased from Fisher Scientific (Thermo Fischer Scientific). 2,2′-Bipyridine-5-carboxylic acid was purchased from HetCat (Basel, Switzerland). *O*-(*N*-succinimidyl)-1,1,3,3-tetramethyluronium tetrafluoroborate (TSTU), borane dimethylamine complex, tetrakis(triphenylphosphine)palladium(0), triethylsilane (TES), acetic anhydride, cupric chloride, and PBS (pH 7.4) were purchased from Sigma-Aldrich.

*Radiolabeling and in vivo imaging*: *S*-2-(4-Isothiocyanatobenzyl)-diethylenetriamine pentaacetic acid (*p*-SCN–Bn-DTPA) was obtained from Macrocyclics (Plano, TX USA). Dimethyl sulfoxide (DMSO), ethylenediaminetetraacetic acid (EDTA) and sodium bicarbonate ($NaHCO_3$) were purchased from Sigma–Aldrich. $^{111}InCl_3$ was cyclotron produced and provided by BWTX (Vancouver, Canada) as a ~ 0.1 M HCl solution. Water was purified using an Ultra Clear Water System (Siemens) set at 0.055 µS cm$^{-1}$.

**Synthesis of the peptide**. The linear peptide sequence was assembled by Fmoc SPPS on an automated Initiator + Alstra™ microwave peptide synthesizer (Biotage, Sweden). The synthesis was carried out on a TentaGel S Rink-amide resin (0.22 mmol/g loading) with 9-fluorenylmethyloxycarbonyl (Fmoc) for protection of $N^{\alpha}$-amino groups except for the *N*-terminal Ile, where Boc (tert-butoxycarbonyl) was used. $N^{\alpha}$-Fmoc deprotection was performed at room temperature in two stages by treating the resin with piperidine/DMF (1:4) for 3 min followed by piperidine/DMF (1:3) for 15 min. The resin was then washed with NMP (3x), $CH_2Cl_2$ (1x) and NMP (3x). Peptide couplings were performed using 5.5 equiv. of $N^{\alpha}$-Fmoc amino acids in DMF (0.5 M), 5.5 equiv. of HOAt in DMF (0.5 M), 5.0 equiv. of HBTU in DMF (0.6 M), and 9.9 equiv. of DIEA in

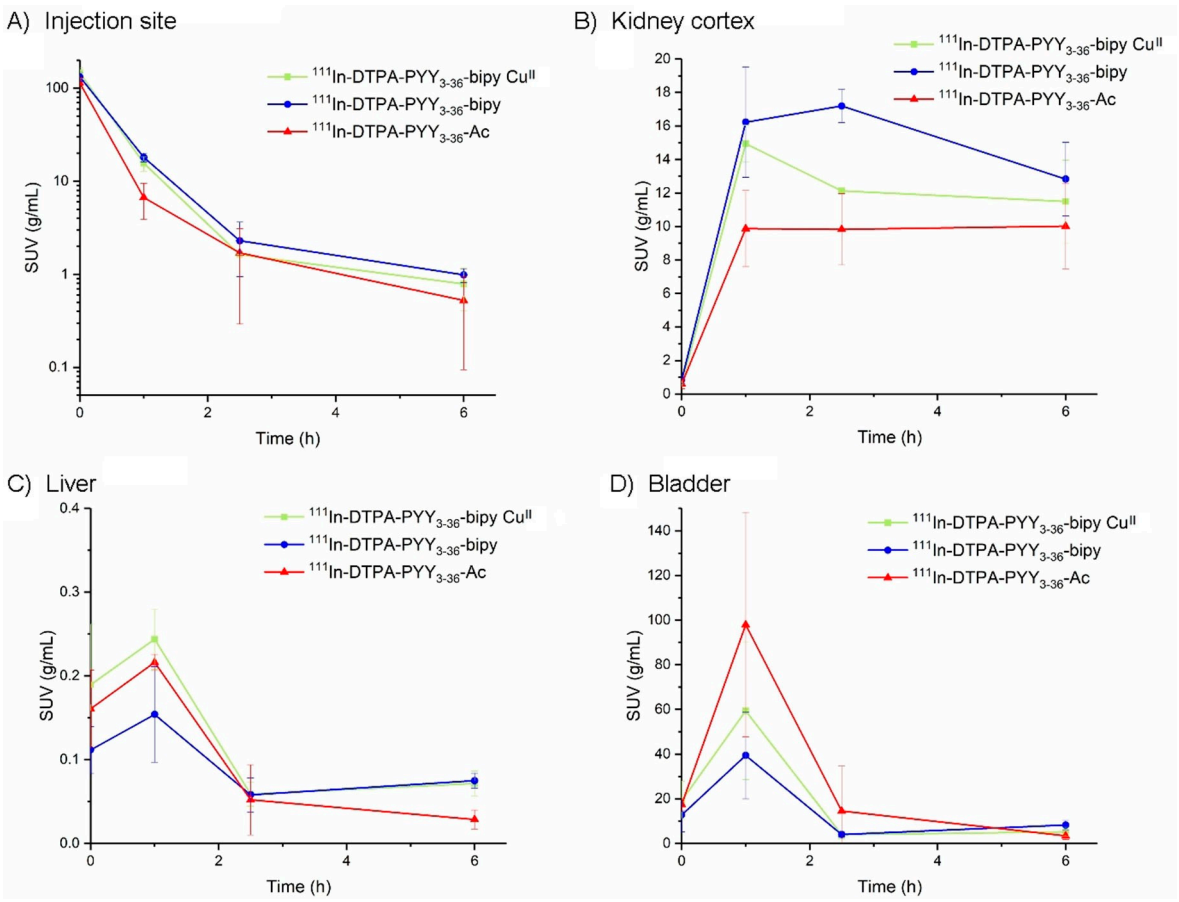


**Figure 6.** Representative SUV time-activity curves for all radioconjugates in mice ($n = 3$).

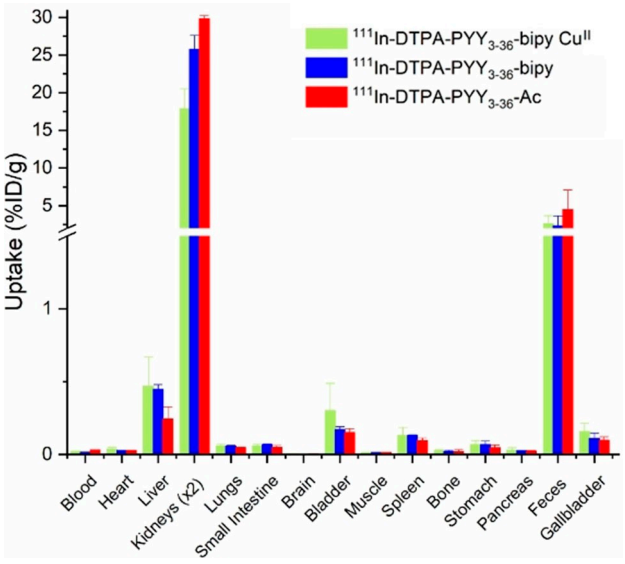


**Figure 7.** Biodistribution of the tested radioconjugates showing organ uptake expressed as %ID/g 24 h post-injection.

NMP (2 M). The coupling time was 10 min at 75 °C, after which the resin was washed with NMP (3x), $CH_2Cl_2$ (1x), and NMP (3x).

**Synthesis of *O*-succinimidyl-2,2′-bipyridine-5-carboxylate.** A mixture of 2,2′-bipyridine-5-carboxylic acid (30 mg; 0.155 mmol) and TSTU (89 mg; 0.297 mmol; 1.92 equiv.) was suspended in dry DMF (0.5 mL). DIEA (50 µL; 0.297 mmol; 1.92 equiv.) was added dropwise to provide a dark-brown solution, which was left stirring at room temperature overnight. Water (5 mL) was added to precipitate the product. After centrifugation, the precipitate was redissolved in MeCN and concentrated to provide a white solid. Yield: 55%; $^1$H NMR (500 MHz; $CD_3CN$): $\delta = 9.33$ (dd, $J = 2.2$, 0.9 Hz, 1H), 8.73 (ddd, $J = 4.8$, 1.8, 0.9 Hz, 1H), 8.62 (dd, $J = 8.4$, 0.9 Hz, 1H), 8.54 (dd, $J = 8.4$, 2.2 Hz, 1H), 8.52 (dt, $J = 8.0$, 1.1 Hz, 1H), 7.97 (td, $J = 7.8$, 1.8 Hz, 1H), 7.48 (ddd, $J = 7.6$, 4.8, 1.2 Hz, 1H), 2.88 ppm (s, 4 H). $^{13}$C NMR (125 MHz; $CD_3CN$): $\delta = 171.0$, 162.2, 162.0, 155.2, 151.7, 150.7, 139.7, 138.4, 126.2, 122.8, 122.2, 121.7, 26.5 ppm.

**Synthesis of PYY$_{3-36}$ analogues.** To synthesize PYY$_{3-36}$ analogues, resin-bound Boc-[R$^4$,K$^7$,W$^{30}$]PYY$_{3-36}$ was selectively elongated at the ε-amine of Lys7 using SPPS. The Alloc group protecting the ε-amine of Lys7 was manually deprotected using 1 equiv. tetrakis (triphenylphosphine)palladium(0) and 1.5 equiv. borane dimethylamine complex in $CH_2Cl_2$, which had been bubbled with argon gas. $CH_2Cl_2$ (10 mL) was added to the resin, and the mixture was flushed with argon for 15 min prior to the addition of the borane dimethylamine complex, followed by an additional 10 min of argon flow. Subsequently, tetrakis(triphenylphosphine)palladium(0) was added and the reaction was left with argon bubbling for 2 h at room temperature. Afterwards, the resin was washed sequentially with $CH_2Cl_2$ (3x), DMF (3x), and $CH_2Cl_2$ (3x). Alloc removal was confirmed by a LC–MS of a test cleavage (10 mg resin) using 2 mL

of 95:2.5:2.5 TFA/TES/$H_2O$ for 2 h at room temperature. The resin was washed with DMF (3x), $CH_2Cl_2$ (3x) and DMF (3x) and it was divided into two portions: Portion i) was acetylated to the ε-amine of Lys7 with 25% $Ac_2O$ in DMF (6 mL) for 2 h at room temperature and portion ii) was coupled to the succinimide ester of bipyridine that was dissolved in 0.02 M DIEA in DMF (3 mL). The latter reaction was shaken for 5 h (150 rpm) at room temperature, after which it was washed with DMF (3x).

**Purification of peptides**. After synthesis, resins were washed with DMF (3x) and $CH_2Cl_2$ (3x). The peptides were released from the solid support by treatment with TFA/$H_2O$/TES (95:2.5:2.5; 10 mL) for 2 h. Following cleavage, the TFA solutions were concentrated by nitrogen flow and the compounds were precipitated with cold diethyl ether to yield the crude product as white powder. Then, the peptides were purified by RP-HPLC on a Dionex Ultimate 3000 system (Thermo Scientific) with a preparative $C_{18}$ column (Phenomenex Gemini, 110 Å 5 μm $C_{18}$ particles, 21.2×100 mm) using the following system: solvent A, water containing 0.1% TFA; solvent B, acetonitrile containing 0.1% TFA. B gradient elution (5–100% over 25 min) was applied at a flow rate of 20 mL $min^{-1}$ and column effluent was monitored by UV absorbance at 215 nm.

**Analysis of peptides**. Identification and quantification were carried out on analytical HPLC on a Dionex Ultimate 3000 system (Thermo Scientific) with a Jupiter $C_4$ column (5 μm, 150×4.6 mm) coupled to a ESI-MS (MSQ Plus Mass Spectrometer, Thermo). The column was eluted using a linear gradient flow of water-acetonitrile containing 0.1% formic acid at a flow rate of 1.0 mL $min^{-1}$.

**UV/vis analysis**. UV/vis spectra were recorded on a Jasco V-650 spectrophotometer using rectangular Hellma quartz cells with a light path of 3.00 mm. The peptide solutions were 100 μM in 0.1 mM PBS pH 7.4 and various concentrations of $CuCl_2$ were added. The solutions were equilibrated overnight at room temperature.

**Dynamic light scattering**. Samples (100 μM in 0.1 mM PBS buffer pH 7.4) were filtered into quartz cuvettes through 0.45 μm filters. The calculated amount of $Cu^{II}$ was added followed by addition of 0.1 mM PBS pH 7.4 (60 μL). The solutions were equilibrated overnight at room temperature. All DLS measurements were performed on a Malvern Zetasizer μV instrument at 25 °C using a quartz cuvette with 1.25 mm light path length. Measurements were obtained as 4 acquisitions of 12–16 cycles, and the size distribution was taken as an average of four repeated measurements. Data were analyzed using the Zetasizer Software v7.11.

**Chelator-modified peptide syntheses**. In two separate vials, $PYY_{3-36}$-bipy and $PYY_{3-36}$-Ac were dissolved with 30% $CH_3CN$ in 0.1 M sodium bicarbonate buffer (500 μL, pH 9) to a final concentration of 2 g/L (0.23 μmol) and the chelator solution of *p*-SCN–Bn-DTPA was added (25 μL, 20 g/L, 4 equiv.). *p*-SCN–Bn-DTPA stock solution was in anhydrous DMSO. The pH of the reaction mixtures was adjusted to pH 8.5–9.0 with $Na_2CO_3$, and the mixtures were incubated overnight at room temperature with agitation (600 rpm). The course of the reaction was monitored by RP-HPLC. After 21 h, the mixtures were purified on a HPLC Waters Alliance e2695 Separations module coupled to a Waters 2489 UV/vis detector. The column was an analytical $C_{18}$ (Waters, Atlantis T3 column, 100 Å, 5 μm particle size, 4.6 x 150 mm) supported by a $C_{18}$ guard cartridge and was operated in an oven (40 °C). Employed mobile phases were 0.1% TFA in water (eluent C) and 0.1% TFA in acetonitrile (eluent D). The linear gradient used was 5–100% of B with a flow rate of 1.00 mL/min over 15 min.

**$^{111}$In radiolabeling of DTPA-$PYY_{3-36}$ analogues**. $^{111}InCl_3$ (47.36 MBq) was added to DTPA-$PYY_{3-36}$-bipy (that was later treated with $Cu^{II}$) in MilliQ water (0.13 g/L in 399 μL), and the reaction mixture was stirred (600 rpm) at room temperature for 1 h. For $^{111}$In labeling of DTPA-$PYY_{3-36}$-bipy without any addition of $Cu^{II}$, $^{111}InCl_3$ (61.05 MBq) was added to MilliQ water (0.13 g/L of the peptide in 405 μL), whereas for $^{111}$In-DTPA-$PYY_{3-36}$-Ac 76.96 MBq was introduced to 405 μL of water and the reactions mixtures were stirred (600 rpm) at room temperature for 1 h. Instant thin layer chromatography (ITLC) showed high labeling efficiency and radiochemical purity of >97% was achieved for the labeled peptides as determined by radio HPLC. The activities were measured using a Capintec CRC-55tR dose calibrator. Finally, 45 μL of 9% saline were added to each of the three reaction mixtures. The activity for each group was equal to 41.44 MBq at the time of injection (decay corrected).

**Radiolabeling efficiency and purity of $^{111}$In-DTPA-$PYY_{3-36}$ conjugates**. The radiolabeling purity was determined by radio-HPLC using the same Waters Alliance e2695 separations module as described above coupled to a LabLogic Scan-Waters RAM radiodetector. The labeling efficiency was measured by ITLC using Biodex Tec-Control chromatography strips (#150-771, dark green) developed with an aqueous EDTA solution as a mobile phase (0.1 M). The $^{111}$In-DTPA-$PYY_{3-36}$-bipy and $^{111}$In-DTPA-$PYY_{3-36}$-Ac conjugates, which have larger molecular weight, would remain at the origin, while the free $^{111}In^{III}$ moves with the mobile phase at the solvent front [Retention factor: $R_f$ ($^{111}$In-DTPA-$PYY_{3-36}$-bipy or $^{111}$In-DTPA-$PYY_{3-36}$-Ac) = 0, $R_f$ (free $^{111}In^{III}$) = 1]. The developed ITLC strips were analyzed on a Packard Cyclone Phosphorimager (Mississauga, ON, Canada) and a photostimulable phosphor plate using the OptiQuant software.

**Stability study**. The complex stability of $^{111}$In-DTPA-$PYY_{3-36}$-bipy and $^{111}$In-DTPA-$PYY_{3-36}$-Ac was determined at different time intervals using ITLC in the presence of 10% of EDTA (0.1 M). Briefly, 1 μL of EDTA solution (pH 7.4, 10 mM) was added to 9 μL of the radiolabeled pure solution (0.02 mM) and mixed at 37 °C and 650 rpm on an Eppendorf thermal shaker. The resultant solutions were incubated for 1 h and 24 h and analyzed by ITLC. To measure EDTA transchelation the radioactive intensities on the ITLC were integrated and compared [$R_f$ ($^{111}$In-DTPA-$PYY_{3-36}$-bipy or $^{111}$In-DTPA-$PYY_{3-36}$-Ac) = 0, $R_f$ (free $^{111}In^{III}$) = 1].

**$Cu^{II}$ complexation**. For copper complexation, 0.5 equiv. of $CuCl_2$ (10 μL; 500 μM stock solution) was added to $^{111}$In-DTPA-$PYY_{3-36}$-bipy in MilliQ water (0.13 g/L in 399 μL) and was left at room temperature to equilibrate overnight.

***In vivo* SPECT/CT imaging**. This study was performed in accordance with the Canadian Council on Animal Care (CCAC) and protocol approved by the Animal Care Committee (ACC) of the University of British Columbia (A16-0150). $^{111}$In-DTPA radioconjugates were prepared as described above on the day prior to the experiment and were stored overnight at 4 °C. On the day of administration, quality control of the radioconjugates was performed by radio-HPLC and ITLC. Healthy 6–8 week-old female C57Bl/6 mice (~20 g) were obtained from Charles River and allowed free access to food and water. The mice were sorted into three groups of three individuals. Mice were anesthetized with isoflurane on a precision vaporizer (5% in oxygen for induction, between 1.5 and 2.5% in oxygen for maintenance) and received a subcutaneous injection (SQ) of lactated Ringer's (0.5 mL) for hydration prior to the last two imaging scans. After the induction of anesthesia, an injection of 100 μL (12 μg) of $^{111}$In-DTPA-$PYY_{3-36}$-bipy $Cu^{II}$, $^{111}$In-DTPA-$PYY_{3-36}$-bipy and $^{111}$In-DTPA-$PYY_{3-36}$-Ac in 0.9% saline was SQ administered to each group, respectively. Average injected activity was 7.4 MBq per mouse. Immediately after injection, the animal was prepared for SPECT/CT imaging. Respiratory rate and temperature were monitored constantly during the scans, and isoflurane and bed temperature adjusted accordingly. Animals were recovered after each scan and euthanized 24 h post-injection by $CO_2$ asphyxiation under isoflurane anesthesia. Cardiac puncture was promptly

performed to recover blood, and the organs of interest were harvested for a full biodistribution.

**SPECT/CT parameters and image reconstruction**. The SPECT/CT imaging was performed using a VECTor/CT preclinical small animal scanner (MILabs, Utrecht, The Netherlands) equipped with an extra ultra-high sensitivity pinhole collimator (XUHS). Immediately after injection, static whole-body images were acquired at 0, 1, 2.5 and 6 h post injection. Static 10 min scans were performed at 0 and 1 h scans, while longer imaging times of 20 min were performed at subsequent imaging time-points (2.5 and 6 h). Following each SPECT acquisition, a whole-body CT scan was acquired to obtain anatomical information and both images were registered. The $^{111}$In photopeak window was centered at 171 keV with a 20% energy window width. CT scans were acquired with a tube setting of 55 kV and 615 μA. In total 2 frames of 180 projections over 360° were acquired in step and shoot rotation mode. The acquired projection data was reconstructed using SkyScan NRecon software to generate a 3D CT image on 0.169 mm$^3$ voxel size. For quantitative analysis, SPECT image reconstructions were carried out with a pixel-ordered subset expectation maximization (POSEM) algorithm[53] that included resolution recovery and compensation for distance-dependent pinhole sensitivity. For the SPECT images, we used 16 subsets, 6 iterations, and an isotropic 0.4 mm voxel grid. The images were decay corrected to the starting scan time, and after CT registration, attenuation correction was applied. For visual representation, the reconstructed volumes of SPECT scans were post-filtered with a 3D Gaussian filter. Volumes of interest (VOIs) were manually defined using the imaging software AMIDE (v.1.0.5)[54] to determine the time-activity pattern per target organ. Thus, the delineated regions were liver, bladder, kidneys and injection site. The average organ activity per volume was obtained from the SPECT images, and the standardized uptake value (SUV) calculated for each organ. In order to relate the scanner units (counts/voxel) to radioactivity concentration, a calibration factor was determined scanning a source with a known concentration of $^{111}$In. Mice were sacrificed for *ex vivo* biodistribution, and the radioactivity in diverse organs was determined by gamma counting.

***Ex vivo* biodistribution**. A complete biodistribution was conducted (blood, heart, liver, kidneys, lungs, small intestine, brain, bladder, muscle, spleen, stomach, pancreas, feces, urine and gallbladder) at 24 h post-injection. The organs were cleaned from blood and weighed, and the radioactivity was measured using a calibrated gamma counter (Packard Cobra II Autogamma counter, PerkinElmer). Total organ weights were used for the calculations of injected dose per gram of tissue (% ID/g organ) except for blood, muscle, and bone, where average literature values were used.[55]

**Statistical analysis**. Data were compiled in Microsoft Excel and evaluated in GraphPad Prism and Excel. All data are expressed as mean ± standard deviation (SD). Outliers were identified via a Grubbs test ($p < 0.05$) and were excluded from the reported results. Statistical analysis for the biodistribution and the standard uptake values of each organ was performed by multiple t-tests assuming equal variance. The difference was considered statistically significant when P value was $< 0.05$.

## Acknowledgements

*The authors acknowledge support from the Novo Nordisk Foundation (Grand Challenge Program; NNF16OC0021948) and the Lundbeck Foundation, Denmark (Joint Professorship to UOH, grant no. 2014-4176). K.S. acknowledges the generous support of BWXT Isotope Technology Group for the supply of the radioisotope. The authors would also like to thank Maryam Osooly for her skillful assistance in the imaging lab, and the Canada Foundation for Innovation (project no. 25413) for its support of the imaging facility (http://invivoimaging.ca/).*

## Conflict of Interest

The authors declare no conflict of interest.

**Keywords:** bipyridine · copper · imaging · indium · peptide synthesis · self-assembly

[1] L. Jorgensen, S. Hostrup, E. H. Moeller, H. Grohganz, *Expert Opin. Drug Delivery* **2009**, *6*, 1219–1230.
[2] D. S. Goodsell, A. J. Olson, *Annu. Rev. Biophys. Biomol. Struct.* **2000**, *29*, 105–153.
[3] Y. Li, Q. Zou, C. Yuan, S. Li, R. Xing, X. Yan, *Angew. Chem. Int. Ed.* **2018**, *57*, 17084–17088.
[4] M. Albrecht, P. Stortz, *Chem. Soc. Rev.* **2005**, *34*, 496–506.
[5] V. Tanchou, F. Gas, A. Urvoas, F. Cougouluègne, S. Ruat, O. Averseng, E. Quéméneur, *Biochem. Biophys. Res. Commun.* **2004**, *325*, 388–394.
[6] E. N. Baker, H. M. Baker, *Biochimie* **2009**, *91*, 3–10.
[7] M. J. Adams, T. L. Blundell, E. J. Dodson, G. G. Dodson, M. Vijayan, E. N. Baker, M. M. Harding, D. C. Hodgkin, B. Rimmer, S. Sheat, *Nature* **1969**, *224*, 491–495.
[8] R. Zou, Q. Wang, J. Wu, J. Wu, C. Schmuck, H. Tian, *Chem. Soc. Rev.* **2015**, *44*, 5200–5219.
[9] R. D. Hancock, A. E. Martell, *Chem. Rev.* **1989**, *89*, 1875–1914.
[10] C. Kaes, A. Katz, M. W. Hosseini, *Chem. Rev.* **2000**, *100*, 3553–3590.
[11] T. Koide, M. Yuguchi, M. Kawakita, H. Konno, *J. Am. Chem. Soc.* **2002**, *124*, 9388–9389.
[12] D. E. Przybyla, J. Chmielewski, *J. Am. Chem. Soc.* **2008**, *130*, 12610–12611.
[13] M. M. Pires, D. E. Przybyla, J. Chmielewski, *Angew. Chem. Int. Ed.* **2009**, *48*, 7813–7817; *Angew. Chem.* **2009**, *121*, 7953–7957.
[14] H. Ishida, Y. Maruyama, M. Kyakuno, Y. Kodera, T. Maeda, S. Oishi, *ChemBioChem* **2006**, *7*, 1567–1570.
[15] M. R. Ghadiri, C. Soares, C. Choi, *J. Am. Chem. Soc.* **1992**, *114*, 825–831.
[16] M. Gochin, V. Khorosheva, M. A. Case, *J. Am. Chem. Soc.* **2002**, *124*, 11018–11028.
[17] W. D. Kohn, C. M. Kay, B. D. Sykes, R. S. Hodges, *J. Am. Chem. Soc.* **1998**, *120*, 1124–1132.
[18] H. K. Munch, S. T. Heide, N. J. Christensen, T. Hoeg-Jensen, P. W. Thulstrup, K. J. Jensen, *Chem. Eur. J.* **2011**, *17*, 7198–7204.
[19] B. P. Gilmartin, K. Ohr, R. L. Mclaughlin, R. Koerner, M. E. Williams, *J. Am. Chem. Soc.* **2005**, *127*, 9546–9555.
[20] M. B. Coppock, J. R. Miller, M. E. Williams, *Inorg. Chem.* **2011**, *50*, 949–955.
[21] P. Holzer, F. Reichmann, A. Farzi, *Neuropeptides* **2012**, *46*, 261–274.
[22] R. L. Batterham, M. A. Cowley, C. J. Small, H. Herzog, M. A. Cohen, C. L. Dakin, A. M. Wren, A. E. Brynes, M. J. Low, M. A. Ghatei, et al., *Nature* **2002**, *418*, 650–654.
[23] R. L. Batterham, M. A. Cohen, S. M. Ellis, C. W. Le Roux, D. J. Withers, G. S. Frost, M. A. Ghatei, S. R. Bloom, *N. Engl. J. Med.* **2003**, *349*, 941–948.
[24] R. A. Lafferty, P. R. Flatt, N. Irwin, *Peptides* **2018**, *100*, 269–274.
[25] S. Østergaard, K. W. C. Frieboes, B. Wieczorek, J. K. Thomsen, B. S. Wulff, C. Jessen, WO 2016/124687 A1, **2016**.
[26] J. Kofoed, L. Ynddal, S. Østergaard, R. Jørgensen, F. Nielsen, C. Nilsson, J. K. Thomsen, WO 2011/058165 A1, **2011**.
[27] S. R. Bloom, WO 2015/177573 A1, **2015**.
[28] S. Østergaard, J. Kofoed, J. F. Paulsson, K. G. Madsen, R. Jorgensen, B. S. Wulff, *J. Med. Chem.* **2018**, *61*, 10519–10530.
[29] G. H. Ballantyne, *Obes. Surg.* **2006**, *16*, 795–803.
[30] J. Olsen, J. Kofoed, S. Østergaard, B. S. Wulff, F. S. Nielsen, R. Jorgensen, *Peptides* **2016**, *78*, 59–67.
[31] S. B. Van Witteloostuijn, S. L. Pedersen, K. J. Jensen, *ChemMedChem* **2016**, *11*, 2474–2495.

[32] E. M. Bech, S. L. Pedersen, K. J. Jensen, *ACS Med. Chem. Lett.* **2018**, *9*, 577–580.
[33] I. Jonassen, S. Havelund, T. Hoeg-Jensen, D. B. Steensgaard, P.-O. Wahlund, U. Ribel, *Pharm. Res.* **2012**, *29*, 2104–2114.
[34] K. J. Jensen, *J. Pept. Sci.* **2013**, *19*, 537–544.
[35] R. Chakrabarty, P. S. Mukherjee, P. J. Stang, *Chem. Rev.* **2011**, *111*, 6810–6918.
[36] M. Irving, D. H. Mellor, *J. Chem. Soc.* **1962**, 5222–5237.
[37] A. E. Martell, R. M. Smith in *Critical Stability Constants, Vol. 5: First Supplement* (Eds.: A. E. Martell, R. M. Smith), Plenum, New York **1982**, 248.
[38] B. Gutfilen, S. A. L. Souza, V. Gianluca, *Drug Des. Dev. Ther.* **2018**, *12*, 3235–3245.
[39] P. Gomez-Martinez, M. Dessolin, F. Guibé, F. Albericio, *J. Chem. Soc. Perkin Trans. 1* **1999**, 2871–2874.
[40] K. Nakamoto, *J. Phys. Chem.* **1960**, *64*, 1420–1425.
[41] C. F. Ramogida, C. Orvig, *Chem. Commun.* **2013**, *49*, 4720–4739.
[42] E. W. Price, C. Orvig, *Chem. Soc. Rev.* **2013**, *43*, 260–290.
[43] S. Liu, D. S. Edwards, *Bioconjugate Chem.* **2001**, *12*, 7–34.
[44] M. W. Brechbiel, O. A. Gansow, *Bioconjugate Chem.* **1991**, *2*, 187–194.
[45] J. S. Ahn, R. Nazarbaghi, L. J. D'Souza, S. Ghosh, C. M. Jodka, A. N. Lwin, O. E. Levy, *Adv. Exp. Med. Biol.* **2009**, *611*, 515–516.
[46] E. M. Bech, A. Kaiser, K. Bellmann-Sickert, S. S. Nielsen, K. K. Sørensen, L. Elster, N. Hatzakis, S. L. Pedersen, A. G. Beck-Sickinger, K. J. Jensen, *Mol. Pharm.* **2019**, *16*, 3665–3677.
[47] J. P. Holland, M. J. Williamson, J. S. Lewis, *Mol. Imaging* **2010**, *9*, 1–20.
[48] J. Blachot, *Nucl. Data Sheets* **2009**, *110*, 1239–1407.
[49] E. Vegt, E. M. Van Eerd, A. Eek, W. J. G. Oyen, J. F. M. Wetzels, M. De Jong, F. G. M. Russel, R. Masereeuw, M. Gotthardt, O. C. Boerman, *J. Nucl. Med.* **2008**, *49*, 1506–1511.
[50] E. I. Christensen, J. Gburek, *Pediatr. Nephrol.* **2004**, *19*, 714–721.
[51] S. Silbernagl, *Physiol. Rev.* **1988**, *68*, 911–1007.
[52] R. P. L. Van Swelm, J. F. M. Wetzels, D. W. Swinkels, *Nat. Rev. Nephrol.* **2020**, *16*, 77–98.
[53] W. Branderhorst, B. Vastenhouw, F. J. Beekman, *Phys. Med. Biol.* **2010**, *55*, 2023–2034.
[54] A. M. Loening, S. S. Gambhir, *Mol. Imaging* **2003**, *2*, 131–137.
[55] H. L. Foster, D. J. Small, J. G. Fox in *The mouse in Biomedical Research, Vol. 3* (Eds.: H. L. Foster, J. D. Small, J. G. Fox), Academic Press, New York **1983**.

Manuscript received: April 30, 2020
Revised manuscript received: July 10, 2020
Accepted manuscript online: July 15, 2020
Version of record online: ■■, ■■■

# FULL PAPERS

**Peptide self-assembly**: Radiolabeling of a re-engineered peptide $YY_{3–36}$ ($PYY_{3–36}$) with a 2,2′-bipyridine ligand enabled higher-order self-assemblies through coordination with $Cu^{II}$. We studied the effect of the self-assembly *in vivo* by using non-invasive quantitative bioimaging. Abiotic ligands might influence the controlled release of biopharmaceuticals from subcutaneous depots.

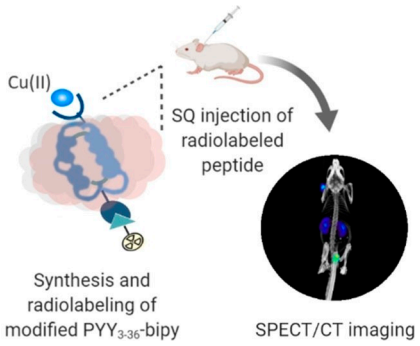


*P. Kalomoiri, Dr. C. Rodríguez-Rodríguez, Dr. K. K. Sørensen, M. Bergamo, Dr. K. Saatchi, Prof. U. O. Häfeli*, Prof. K. J. Jensen**

1 – 12

**Bioimaging and Biodistribution of the Metal-Ion-Controlled Self-Assembly of $PYY_{3–36}$ Studied by SPECT/CT**